Volume 1 | Number 1 | Jan 2013 | Pages 1–100

Journal of
Materials Chemistry A

Materials for energy and sustainability
www.rsc.org/materialsA

ROYAL SOCIETY
OF CHEMISTRY

ROYAL SOCIETY
OF CHEMISTRY

www.rsc.org/materialsA

Journal Name

ARTICLE TYPE

Porous imine-based networks with protonated imine linkages for carbon dioxide separation from mixtures with nitrogen and methane

Nadine Popp[a], Thomas Homburg[b], Norbert Stock[b], Jürgen Senker*,[a]

Porous imine-linked networks (PINs) have been prepared by catalyst-free Schiff base condensation reaction of 2,4,6-(4-aminophenyl)1,3,5-triazine with 9,10-anthracene-dicarboxaldehyde (PIN1 and PIN1_2) and with 4,4`,4``,4```-methanetetrakis-benzaldehyde (PIN2). Even after synthesis optimisation, only with DMSO (PIN1 and PIN2) microporous frameworks were obtained, whereas DMF (PIN1_2) and
10 other solvents lead to nonporous systems, estimated by argon measurements. Furthermore, ^{15}N solid state NMR and IR spectroscopy reveal the influence of decomposition products of DMSO leading to protonation of the imine linkage and resulting in an ionic structure with an incorporated sulfonic counterion. Up to now, protonation of an imine function due to the usage of DMSO as solvent has not been discussed in the literature. In contrast, for PIN1_2 the imine linkage remains neutral. Argon sorption
15 isotherms for PIN1 and PIN2 exhibit surface areas of 458 m^2 g^{-1} and 325 m^2 g^{-1} and the pore structure displays micro- and small mesopores with pore diameters from 0.6 to 5 nm. Additionally, CO_2 isotherms at 273 K demonstrate ultramicropores for all three polymers with similar pore size distributions. Despite the different network structures similar CO_2 uptakes (1.8-1.06 mmol g^{-1} at 273 K at 1.0 bar) and heat of adsorption Q_{st} values of 30 kJ mol^{-1} were obtained. In line with the polyionic character of PIN1 and PIN2
20 both compounds adsorbs three times more water than the more hydrophobic, neutral PIN1_2 at room temperature indicating two different adsorption mechanisms. IAST selectivity calculations show good CO_2/N_2 (30-31) and CO_2/CH_4 (8-12) selectivity factors. Despite to their moderate BET-surface areas, the PINs show good CO_2 uptakes and selectivity factors.

25 Some recent forecasts suggest that the global primary energy demand will rise by 53 % in the period 2004-2030.[1] To supply the energy especially for industrial activities fossil flue still remains with a contribution of 85 % the dominant source.[2] About 40 % of the energy-related CO_2 emission comes from coal-, oil or
30 natural gas-fired power plants.[1,3] The continuous growth in energy demands fossil flue combustion to remain a dominant component despite the rapid expansion of renewable energy sources such as wind, solar, and bio-flue power.[4,5] This leads to an urgent need for strategies to reduce global carbon dioxide
35 emissions. One potential approach is the carbon capture and storage (CCS). CCS contains carbon capture as well as transport and long time storage by geological sequestration or the further utilization of CO_2.[2,5] One major drawback of this approach is the high costs of capturing CO_2 in today`s technologies.[6] The
40 application field for capturing CO_2 is divided into post-combustion and pre-combustion processes.[7] In post-combustion for example flue gas in power plants a separation of CO_2 from mainly N_2 and H_2O is required. A typical flue gas is composed of 15-16 % CO_2, 70-75 % N_2, 5-7 % H_2O and some additional
45 impurities.[5]
The separation of CO_2 from CH_4 or H_2 in the pre-combustion process is employed in natural gas sources or water-gas shift

reactors. Sources such as natural gas and landfill gas are contaminated with about 10 % and 40-60 % carbon dioxide,
50 respectively. The so called "sweetening" of CH_4, as a less CO_2 emitting energy source, is essential to increase energy density and to avoid pipeline corrosion caused by the acidic CO_2.[8]
Industrial processes for capturing CO_2 are still based on the application of aqueous amine solutions.[9] However, amine
55 scrubbing has some major disadvantages.[2,7] The need of large amounts of solvents, the high regeneration temperature and the formation of toxic byproducts as well as the high consumption of water raises the costs in CCS for power plants. Furthermore, the separation process might consume between 25 and 40% of the
60 fuel energy of a power plant.[5] One alternative method represents the process of reversible physisorption between nanoporous solid adsorbents and CO_2. The reversible process requires less energy compared to the conventional techniques mentioned above.[10,11,12] Many porous materials such as activated carbon[13], zeolithes[14,15],
65 metal organic frameworks[16,17,18] and porous organic polymers[19,20] were excessively studied for CCS.
The synthetic diversity for tuning the structure and, furthermore, the chemical and physical stability in harsh environments in comparison with other porous solids make porous organic
70 polymers (POPs) one of the most promising classes for CO_2

storage and separation. Various kinds of POPs are currently reported in the literature such as covalent triazine frameworks (CTFs),[21,22] covalent organic frameworks (COFs),[23,24] benzimidazole-linked polymers (BILPs),[25,26] polymers with intrinsic microporosity (PIMs),[27,28] carbazol-based porous polymers (CPOPs),[29,30] porous polyimide networks,[31,32,33] and azo-linked porous organic polymers.[34,35] Among these examples, porous frameworks containing C-N linkages are particularly attractive materials for capturing CO_2, due to their dipole-dipol interaction ($N(\delta^-)\cdots(\delta^+)CO_2$). One possibility for incorporating such as functional groups is Schiff base chemistry (C=N) using amines and aldehydes as monomers. The attractiveness of this reaction is based on a simple condensation reaction excluding the need of any kind of metal catalyst and without formation of toxic byproducts.[36] Furthermore, crystallinity could be achieved due to the reversibility of the reaction. The advantages of highly ordered systems are similar pore sizes and an easy tunability of pore shape and size. In 2009, Uribe-Romo *et al.* reported a new class of crystalline networks by synthesizing COF300 from terephthal-aldehyde and tetra(4-anilyl)methane.[24] For this imine-linked polymer a surface area of 1360 m^2g^{-1} was observed and the pore size distribution showed mainly pores with a size around 0.78 nm. In addition to this crystalline polymer, several amorphous porous Schiff base networks with high surface areas for gas storage and separation have been published. For example, Pandey *et al.* synthesized polymeric organic frameworks (POFs) via Schiff base condensation between 1,3,5-triformylbenzene and diamine monomers.[37] These polymers exhibit high specific surface areas (up to 1500 m^2g^{-1}) and a promising H_2 adsorption capacity. Furthermore, the effect of the solvent on the surface area was described in this work. High polarity solvents (DMSO, DMF) prevent any premature precipitation in contrast to low polar solvents (mesitylene, dioxane) and, therefore, a high cross-linking degree of the network could be achieved. Inspired by Schiff base chemistry the synthetic strategy using melamine or 2,6-diaminopyridine leads to formation of an aminal.[38,39,40,41] The usage of this *N*-hetero-aromatic amines leads to materials with high nitrogen contents up to 40 %. The incorporation of heteroatoms by using triazine units is expected to lead to higher CO_2 adsorption. The basic nitrogen sites of the triazine units in combination with generated imine groups may serve as specific adsorption sites enhancing the CO_2 uptake. This might increase the capacity for capture CO_2. It could be shown that the insertion of triazine units instead of phenyl nodes into the network CMP-5 increased the capability to capture CO_2 by 55 % at 298 K.[42]

In this study, we present the synthesis and characterization of two porous imine networks (PINs). Both are based on 2,4,6-(4-aminophenyl)1,3,5-triazine as the main building block. The synthesis has been complemented with using sterical demand aldehydes to prevent a entirely planar arrangement and therefore an efficient packing of the network. For this, we used 9,10-anthracene-dicarboxaldehyde and 4,4`,4``,4```-methanetetrakis-benzaldehyde in our systems. The polyimines were prepared by a catalyst free condensation reaction in DMSO as solvent. We examine the influence of DMSO on the generation of porosity and the solvent induced modification of the imine functional group due to decomposition products of DMSO. Structural and chemical composition of the networks were investigated via infrared and solid-state NMR spectroscopy as well as elemental analysis. Furthermore, material properties concerning surface area, gas storage and selectivity were determined via argon, nitrogen, CO_2, CH_4 and H_2O sorption isotherms.

Experimental section

Methods and Materials

Chloroform, toluene and dimethylsulfoxide were freshly distilled and dried prior usage. All other chemicals were purchased and used without further purification if not explicitly mentioned. All polymerization reactions were carried out under argon atmosphere.

Argon sorption measurements were performed on a Quantachrome Autosorb-1 at 87.3 K. All samples were degassed at 423 K for 20 h under reduced pressure before measurements. For BET calculations the pressure ranges were chosen considering analysis methods for microporous materials.[43] Specific surface areas, pore volumes and pore size distributions (PSD) from the argon isotherms were calculated using QSDFT for carbon materials. For PIN1 the cylindrical pores and adsorption branch model and for PIN2 the slit pores and equilibrium model were used. These models were chosen on the basis of the best fitting error (PIN1: 0.346 % and PIN2: 0.270 %). For estimating the PSD only the adsorption isotherms were used, to avoid artificial peaks. Carbon dioxide, methane and nitrogen measurements were carried out on a Quantachrome Nova surface analyzer. Specific surface areas, pore volumes and pore size distributions from the CO_2 isotherms at 273 K were calculated using a NLDFT slit pore model for carbon materials. The isosteric heat of adsorption was calculated from the CO_2 adsorption isotherms at temperatures of 273 K, 298 K and 313 K by using the Quantachrome ASiQ v3.0 software package.

The water vapor measurements were carried out by a volumetric technique using a BELSORP-max apparatus. The isotherms were recorded up to 90 % RH. The equilibrium time for each RHvalue was set to 600s. The guaranteed pressure fluctuations being not higher than 0.3 %. Before measuring the samples were degassed under reduced pressure for 12 h at 150 °C.

Attenuated total reflectance infrared (ATR-IR) spectroscopy measurements were done on a Jasco FT/IR-6100 spectrometer between 400 and 4000 cm^{-1}. The spectrometer was equipped with a PIKEGladiATR accessory and the spectra were measured at room temperature with a resolution of 4 cm^{-1}. Elementary analysis (CHN) was carried out on a Vario elementar EL III.

All solid-state NMR measurements were performed under magic angle spinning on Bruker Avance II and Avance III HD spectrometers (proton frequencies of 300 MHz, 400 MHz and 600 MHz) at room temperature. More experimental details are shown in the supporting information. For all measurements ZrO_2 rotors were used. The spectra were referenced with respect to TMS for ^{13}C and nitromethane for [15]N. The SPINAL64[44] sequence was used for broadband proton decoupling. For all spectra MAS cross-polarization (CP) experiments, a ramped ^{1}H contact pulse with different contact times was applied (Table S1). Liquid-state NMR spectra were recorded using a Varian INOVA 300 spectrometer operating at 300 MHz. Chemical shifts are reported in ppm relative to the deuterated solvent which was used. All liquid NMR spectra are shown in the supporting

information (Fig S1a, Fig S1b)

Powder X-ray diffraction (PXRD) was measured on a Panalytical Xpert-Pro diffractometer (Bragg-Brentano geometry) equipped with an X`Celerator Scientific RTMS detector. The measurements were carried out by using Nickel filtered Cu-Kα radiation with a wavelength of 1.54187 Å. The samples were placed on a zero background silicon plate spinning with a rotation speed of 1 Hz.

Synthesis of 2,4,6-Tris(4-bromophenyl)-1,3,5-triazine[45]

A solution of trifluormethanesulfonic acid (10.0 g, 66.7 mmol) in dry chloroform (150 mL) was cooled down to 0 °C under argon. Bromobenzonitrile (6.00 g, 33.0 mmol) was added in small portions. After this addition, the mixture was stirred for 1 h at 0 °C and further for 24 h at room temperature. To quench the reaction, 200 mL of water was added and a white precipitate was formed. After stirring for 1 h, the suspension was filtered and the residue was washed with water. The crude product was recrystallized in toluene and dried at 150 °C to yield a white solid. (4.78 g, 8.75 mmol, 26 %). δ_H (300 MHz; CDCl$_3$) 8.63 (d, J = 8.3 Hz, 6H, Ar-H), 7.73 (d, J = 8.3 Hz, 6H, Ar-H). FT-IR (ATR, 4000-400 cm^{-1}) 1590, 1578, 1540, 1512, 1484, 1400, 1368, 1352, 1171, 1066, 1008, 842, 802. EA, Calc. for $C_{12}H_{12}Br_3N_3$ (%): C; 46.19; H, 2.22; N, 7.70. Found: C, 45.35; H, 1.92; N, 7.82.

Synthesis of 2,4,6-Tris(4-aminophenyl)-1,3,5-triazine[46]

A solution of P(t-Bu)$_3$ (10 wt% in hexane, 1.05 mmol, 3.12 mL) and Bis-(dibenzylideneaceton)-palladium (602 mg, 1.05 mmol) in dry toluene (80 mL) was stirred at room temperature under argon atmosphere for 10 min. Afterwards 2,4,6-tri(4-bromophenyl)-1,3,5-triazine (5.68 g, 10.47 mmol) and a solution of lithium bis(trimethylsilyl)amide (1 M, 34.30 mL, 34.36 mmol) were added. The mixture was heated up to 80 °C and stirred for 48 h. The brown suspension was cooled to room temperature and quenched with aqueous hydrochlorid acid afterwards. (1 M, 40 mL), diluted with water (50 mL) and diethyl ether (50 mL). The suspension was filtered and the aqueous phase was washed with diethylether (2x50 mL). The aqueous phase was treated with sodium hydroxide solution (1 M) until a yellow precipitate was formed. After filtration, the pale yellow solid was purified by recrystallisation with NMP (N-methylpyrrolidone) and was dried under reduced pressure at 100 °C to yield a yellow solid. (2.68 g, 7.56 mmol, 72 %), δ_H (300 MHz; DMSO-d$_6$) 8.51 (d, J = 8.7 Hz, 6H, Ar-H), 6.82 (d, J = 8.7 Hz, 6H, Ar-H); 5.34 (s, 6H, NH$_2$). δ_c (300 MHhz; DMSO-d$_6$) 169.9 (N=C), 153.4 (C-NH$_2$), 130.6 (Triazine-C$_q$-CH), 123.3 (Triazine-C$_q$), 113.6 (NH$_2$-C$_q$-CH); FT-IR (ATR, 4000-400 cm^{-1}) 3460, 3377, 3317, 3206, 1632, 1604, 1575, 1492, 1428, 1363, 1293, 1177, 1146, 1127, 850, 810. EA Calc. for $C_{21}H_{18}N_6$ (%): C, 71.17; H, 5.12 ; N, 23.71. Found: C, 69.50; H, 4.97; N, 21.75.

Synthesis of 9,10-Anthracenedicarbaldehyde[47]

To a suspension of 9,10-dibromoanthracene (4.77 g, 13 mmol) in 200 mL of dry diethylether n-butyllithium (16,9 mL, 27 mmol) was added at -78 °C. After stirring for 30 min at this temperature, the reaction mixture was allowed to warm up to room temperature. The solution was cooled down again to -78 °C after

1 h and DMF (4 mL, 52 mmol) was added drop-wise. The mixture was allowed to warm up over night, the mixture was diluted with water (15 mL). The resulting precipitate was filtered and washed with water several times. The crude product was purified by recrystallisation in DMSO to obtain orange needles. (1.55 g, 6.6 mmol, 51 %), δ_H (300 MHz; DMSO-d$_6$) 11.47 (s, 2H, -CHO), 8.80 (dd, J = 6.9, 3.3 Hz, 4H, Ar-H), 7.78 (dd, J= 6.9, 3.3 Hz, 4H, Ar-H; δ_c (300 MHz; CDCl$_3$) 194.3 (-CHO), 131.6 (CHO-C$_q$), 130.1 (C$_q$-Aryl), 128.4 (CHO-C$_q$-C$_q$-CH-CH), 124.2 (CHO-C$_q$-C$_q$-CH-CH); FT-IR (ATR, 4000-400 cm^{-1}) 1670, 1541, 1524, 1483, 1439, 1392, 1344, 1275, 1247, 1178, 1164, 1044, 1017, 954, 888, 798, 728. EA Calc. for $C_{12}H_{12}Br_3N_3$ (%): C, 82.04; H, 4.43; Found: C, 76.31; H, 3.96.

Synthesis of Tetraphenylmethane[48]

Chlorotriphenylmethane (5 g, 17.94 mmol) and aniline (4.48 mL, 49.16 mmol) were heated up to 190 °C under vigorous stirring. After approximately 5 min the liquid reaction mixture converted to a solid, which was cooled down to room temperature. Then 2 M HCl (20 mL) and methanol (20 mL) were added to the pulverized solid and the suspension was heated up to reflux for 30 min. The solid was filtered off and washed severeral times with water. The dry solid was suspended in ethanol (200 mL) and cooled down to -10 °C. Then sulfuric acid (96 %, 5.4 mL) and isoamyl nitrite (3.57 mL, 26.55 mmol) were added drop wise and was stirred at -10 °C for 1 h. Hypophosphoric acid (10.64 mL, 0.2 mol) was added slowly and the reaction mixture was heated up to 80 °C. When no gas evolution was observed anymore, the reaction was cooled down. The solid was filtered off and washed subsequently with DMF, water and ethanol. After drying in vacuo (50 °C, 24 h) a beige powder was obtained. Further purification was not necessary. (5.05 g, 15.75 mmol, 87 %). δ_H (300 MHz; CDCl$_3$) 7.20-7.08 (m, 20H, Ar-H. δ_c (300 MHz; CDCl$_3$) 147.0 (C$_q$-C$_q$-C$_o$H), 131.4 (C$_o$H), 127.7 (C$_p$H), 126.1 (C$_m$H), 63.9 (C$_q$). FT-IR (ATR, 4000-400 cm^{-1}) 3083, 3057, 3028, 1592, 1490, 1444, 1183, 1083, 1082, 1034, 1001, 891, 765, 749, 700, 633. EA. Calc. for $C_{25}H_{20}$ (%): C, 93.71; H, 6.29; Found: C, 90.52; H, 6.17.

Synthesis of Tetrakis(4-bromophenyl)methane[48]

Tetraphenylmethane (1.5 g, 4.68 mmol) was cooled down to 0 °C in an ice bath. Under vigorous stirring, bromine (4.83 mL, 93.6 mmol) was added dropwise to the reagent. The evolution of gaseous hydrobromic acid showed the successful conversion. After full addition of the bromine the mixture was stirred for 30 min at 0 °C and then cooled down to -78 °C. At this temperature, ethanol (100 mL) was added and the reaction mixture was allowed to warm up to room temperature overnight. For reduction of excess bromine, the mixture was treated with an aqueous sodium bisulfate solution. After this, the precipitate was filtered and washed additionally with sodium hydrogen sulfate solution and water. The crude material was recrystallized from chloroform/ethanol (1:1) to afford a yellow solid. (1.82 g, 2.9 mmol, 62 %), δ_H (300 MHz; CDCl$_3$) 7.40 (d, J = 8.7 Hz, 8H, Ar$_m$-H), 7.02 (d, J = 8.7 Hz, 8H, Ar$_o$-H). δ_c (300 MHz; CDCl$_3$) 144.7 (C$_q$-C$_q$-C$_o$H), 132.7 (Br-C$_q$-CH-CH), 131.3 (Br-C$_q$-CH-CH), 121.1 (C$_q$-Br), 63.9 (C$_q$). FT-IR (ATR, 4000-400 cm^{-1}) 1477, 1395, 1186, 1077, 1007, 948, 911, 833, 809, 753, 531, 507.

EA. Calc. for $C_{25}H_{16}Br_4$ (%): C, 47.21; H, 2.54; Found: C, 41.89; H, 2.11.

Synthesis of Tetrakis(4-formylphenyl)methane[49]

A solution of Tetrakis(4-bromophenyl)methane (1.82 g, 2.86 mmol) in THF (150 mL) was cooled down to -78 °C. Under stirring a solution of *n*-butyllithium (1.6 *M* in hexane, 26 mmol) was added dropwise. The mixture was kept for 30 min at -78 °C and then anhydrous dimethylformamide (DMF) (4.21 mL, 52 mmol) was added. The resulting green suspension was allowed to warm up to room temperature over night. The milky solution was treated with 1 *M* HCl until the mixture became acidic. The clear solution was extracted with ethyl acetate; the organic phase was washed twice with water and dried over $MgSO_4$. After filtration the volatiles were removed under reduced pressure. The crude yellow product was further purified by chromatography via a column using silica gel (acetone/*n*-hexane 1:1). (0.55 g, 1.28 mmol, 44.8 %), δ_H (300 MHz; CDCl₃) 10.02 (s, 4H, -CHO), 7.85 (d, J = 8.4 Hz, 8H, Ar$_m$-H), 7.44 (d, J = 8.4 Hz, 8H, Ar$_o$-H). δ_c (300 MHz; CDCl₃) 191.6 (-CHO), 151.3 (C_q-C_{qaryl}), 135.1 (CHO-$C_{q,aryl}$), 131.4 (C_q-C_{qaryl}-*CH*), 129.9 (CHO-$C_{q,aryl}$-*CH*), 67.3 (C_q). FT-IR (ATR, 4000-400 cm⁻¹) 3544, 3370, 2841, 2741, 1692, 1597, 1572, 1419, 1389, 1312, 1212, 1166, 1012, 806. E.A. Calc. for $C_{29}H_{20}O_4$ (%): C, 80.54; H, 4.66; Found: C, 75.00; H, 5.54.

General synthesis procedure for polyimine networks

An equimolar ratio of the amine and aldehyde functional groups was chosen. The monomer concentrations for all polymerizations were fixed at 1 wt %. The exact used amounts of monomers, reaction temperature and solvent are summarized in Table 1.

The polymerization was carried out in a dry Schlenk flask equipped with a stirrer and an internal thermometer. To a solution of the aldehyde monomer in DMSO, the amine monomer in DMSO was added dropwise under stirring at room temperature. After complete addition, the reaction mixture was stirred with a specific temperature protocol (Table 1) each temperature step was held for 24 h. Finally the system was cooled down and the resulting solid was filtered and washed with acetone. For purification, the polymer was extracted in a Soxhlet apparatus with tetrahydrofuran for 72 h and dried at 150 °C for 24 h under vacuum.

Table 1 Monomer quantity, solvent and temperature process.

	Monomers	**Solvent**	**Temperatur**
PIN1	0.18 g (0.79 mmol) 9,10-Diformylanthracene 0.19 (0.52 mmol) Tris(4-aminophenyl)-triazine	DMSO (35.5 mL)	25°C, 50°C, 70 °C, 100 °C, 180°C
PIN2	0.18 g (0.42 mmol) Tetrakis(4-formylphenyl)methane 0.20 g (0.56 mmol) Tris(4-aminophenyl)triazine	DMSO (34.5 mL)	25°C, 50°C, 70 °C, 100 °C, 180°C
PIN1_2	0.20 g (0.85 mmol) 9,10-Diformylanthracene 0.20 (0.56 mmol) Tris(4-aminophenyl)-triazine	DMF (42 mL)	25°C, 50°C, 70 °C, 100 °C, 150°C

Synthesis of benzylideneaniline (imine model compound)

Benzaldehyde (5 g, 47.1 mmol) was mixed with aniline (4.3 mL, 47.1 mmol) in 200 mL DMSO. After stirring for 24 h under reflux, the reaction mixture was allowed to cool down to room temperature. The solution was concentrated and dried under reduced pressure. No further purification was used. For protonation of the imine compound benzylideneaniline was dissolved in DMSO and several drops of trifluoroacetic acid were added. The solution was stirred at room temperature for 5 h. The resulting dark reaction mixture was concentrated under reduced pressure and dried at 100 °C under vacuum.

For benzylidenaniline:

(7.24 g, 40.0 mmol, 85 %), δ_H (300 MHz; DMSO-d₆) 8.62 (s, 1H, -CH=N), 7.98-7.96 (m, 2H, Ar-H), 7.57-7.51 (m, 3H, Ar-H), 7.45-7.42 (m, 2H, Ar-H), 7.30-7.25 (m, 3H, Ar-H). δ_C (300 MHz; DMSO-d₆) 161.2 (C=N), 151.9 (136.4(N=C-C_q), 131.9 (N=C-C_pH), 129.7 (N=C-C_oH), 129.3 (C=N-C_mH), 129.2 (N=C-C_mH), 126.5 (C=N-C_pH), 121.5 (C=N-C_oH). FT-IR (ATR, 4000-400 cm⁻¹) 3059, 2888, 1623, 1589, 1575, 1482, 1449, 1365, 1314, 1190, 1170, 1072, 1021, 986, 976, 921, 904, 865, 753, 690. EA Calc. for $C_{13}H_{11}N$ (%): C, 86.15; H, 6.12; N, 7.73; Found: C, 86.04; H, 6.10; N, 7.77.

Synthesis and characterization
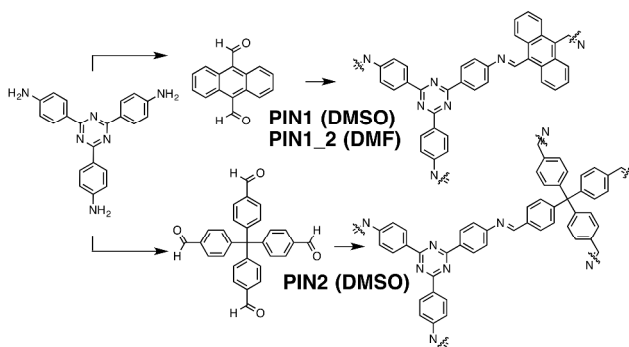
Fig 1 Synthesis route of PIN networks.

PIN1, PIN2 and PIN1_2 were synthesized by a Schiff base condensation reaction of 2,4,6-tris(4-aminophenyl)-1,3,5-triazine with 9,10-anthracenedicarboxaldehyde or tetrakis(4-formyl-phenyl)methane (Fig. 1). The concentration was varied between 0.5-2 % and it turned out that a concentration of 1 wt% for the starting materials and a molar ratio of 1:1 for the functional groups yielded the best surface areas. Furthermore, with DMSO as solvent, the slow addition of the monomers and a temperature gradient, the highest surface areas were obtained. Further solvents such as DMF and NMP were tested. Using these solvents resulted in either no polymers or networks with no and minor porosity, respectively.

The reaction conditions, such as monomer concentration, solvent, reaction time and the reaction process were the key factors for a successful generation of porous materials. To receive a high degree of condensation a slow reaction process in terms of slow addition of the reactants and a continuous increase of temperature in steps are necessary (compare experimental section).[37,50]

Using a solvent with a high boiling point and high polarity e.g. DMSO stimulates cross-linking and prevents premature precipitation of low-polymerized imine oligomers.[37] The reaction

mixtures with DMSO became dark suspensions during the heating process. This is probably a result of the instability of DMSO over the long period of heating.[51,52]

To gain structural information about the polymers, FT-IR as well as [5] ^{13}C and ^{15}N solid-state NMR spectroscopy were acquired. The FT-IR spectra of PIN1/PIN1-2 and PIN2 (Figs. 2 and S2) show characteristic bands at 1500 cm^{-1} (C-N stretching) and 1350 cm^{-1} (in-plane stretching). The ^{13}C and ^{15}N spectra (Fig. 3) show intense peaks at 170 ppm (^{13}C NMR, Fig 3 top) and at -132 ppm [10] (^{15}N NMR, Fig 3 bottom) corroborating a successful incorporation of triazine into the network.[32,53,54,55,56]

In FT-IR spectra, a weak band at 3330 cm^{-1} (Fig S2) and in ^{15}N NMR spectra a signal at -310 ppm were observed. Both are indications of unreacted NH$_2$ groups. The estimation of the [15] amount the amino end groups in ^{13}C NMR spectra is difficult, due to the similar chemical shift of the aromatic carbon adjacent to the imine bond and the NH$_2$ group. Nevertheless, the signal at 192 ppm in ^{13}C NMR and the band in FT-IR at 1680 cm^{-1} (Fig 2) can be assigned to the carbonyl carbon (C=O) of remaining [20] unreacted aldehyde. This is a clear sign that a full conversion into the imine polymer couldn`t be obtained. Although a quantification of the imine formation is not possible due to the nature of the NMR excitation, the nevertheless weak signal intensities indicate high crosslinking degrees for all three [25] networks which we estimate to larger than 80%. This is in agreement with values reported for other polymers.[57,50,37].

In the case of PIN1_2 in FT-IR a typical stretching bond of about 1625 cm^{-1} could be observed. The polymers PIN1 and PIN2, both synthesized in DMSO show in FT-IR spectra no stretching band [30] at about 1620 cm^{-1}. Fig. 2 displays a strong and broad band at 1670 cm^{-1}. This stretching band overlaps with the signal at about 1700 cm^{-1} corresponding from the C=O unit. In the ^{15}N-NMR spectra two new signals at about -250 ppm and -336 ppm occur, whereas the signal at -35 ppm – characteristic for the imine [35] linkage – completely disappears (Fig. 3).
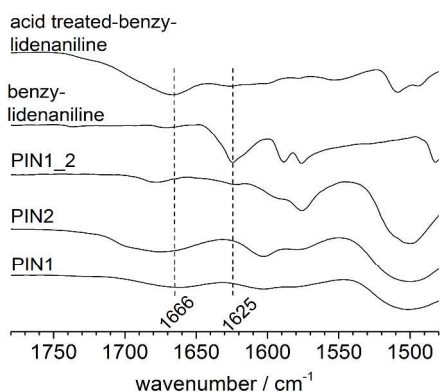
Fig 2 Zoom in (1780-1480 cm^{-1}) of the FT-IR spectra of PIN1, PIN2, PIN1_2, benzylidenaniline and acid-treated-benzylideneaniline.

The occurrence of the new signals in FT-IR spectra and the ^{15}N- [40] NMR spectra suggests a protonation of the imine bond (C=NH$^+$). In order to verify this assumption, a model compound benzylideneaniline was synthesized from aniline and benzaldehyde. Afterwards it was treated with trifluoroacetic acid to obtain a protonated imine compound (acid-treated [45] benzylideneaniline). The conversion was confirmed by FT-IR and

^{13}C-NMR and ^{15}N-NMR studies. In FT-IR (Figs. 2 and S3) the strong characteristic C=N stretching band at 1625 cm^{-1} of benzylidenanilin decreases significantly after addition of the acid, whereas a new band at 1660 cm^{-1} is formed. A decomposition of [50] the imine bond can be excluded because of the absence of the C=O stretching band at 1696 cm^{-1}, which corresponds to the used educt. Additionally, the ^{15}N NMR resonance for the imine group at 18 ppm shifts to -245 ppm after adding trifluoroacetic acid. To probe the proximity of the C=NH$^+$ unit and the trifluoroacetate [55] ^{19}F-^{13}C CP NMR spectra (Fig. S4) were acquired. The acid-treated benzylideneaniline exhibits peaks at 117 ppm and 156 ppm which are ascribed to the trifluoromethyl unit and the carbonyl group of trifluoroacetate, respectively. Additionally, the carbon signals for the imine group (162 ppm) and the aryl units [60] (129 ppm) of protonated benzylideneaniline ions are observed demonstrating a close vicinity of both species. This indicates that an ion pair is formed consisting of a protonated imine unit and trifluoroacetate.

[65]
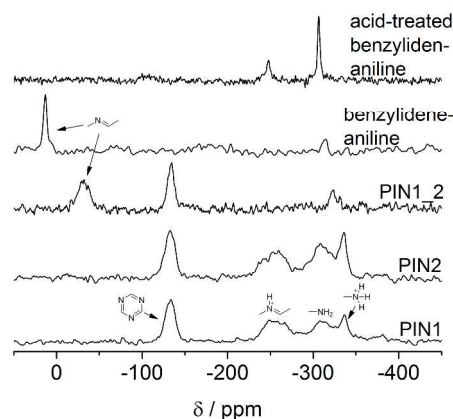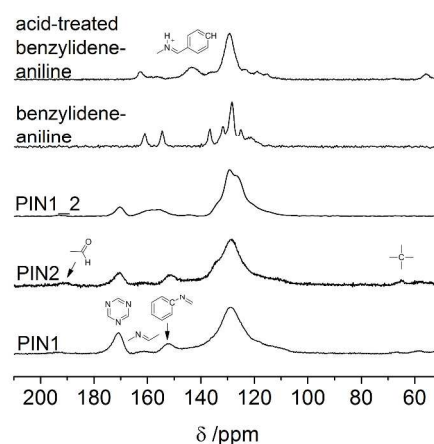
Fig 3 (Top)^{13}C-CP-MAS NMR spectra and (bottom) ^{15}N-CP-MAS NMR spectra of PIN1, PIN2, PIN1_2, benzylidenaniline and acid-treated benzylideneaniline

A comparison of the ^{15}N NMR spectra (Fig 3) of PIN1 and PIN2 [70] with the acid treated benzylidenaniline model compound enables an assignment of the newly formed signals to protonated imine linkage (-250 ppm). Since the signal around -35 ppm, characteristic for the neutral imine unit, completely disappears,

we expect almost quantitative protonation of the latter one. The signal at -336 ppm in PIN1 and PIN2 is consistent with the protonation of unreacted amine groups to NH_3^+ under acidic conditions.[58] On account of the structural equality of the networks PIN1 and PIN1_2, we assume an influence of DMSO as solvent, in particular its decomposition products, in creating such acidic environments. It is known that DMSO is not stable for a long periods of heating at high temperatures, which leads to decomposition products such as formaldehyde, dimethyl sulfide, bis methylthiomethane and methyl disulfide. Furthermore, it was found that DMSO produces acidic species during this decomposition.[52,59] Therefore, as in the case of the model compound, we expect the formation of ion pairs consisting of $C=NH^+$ units and the anionic decomposition products of DMSO for PIN1 and PIN2. This hypothesis if furthermore substantiated by elemental analysis (Table 2). The CHNS analysis yield a significant sulphur content of PIN1 and PIN2 of 2.71 % and 2.94 %, respectively, whereas for PIN1_2 no sulphur was observed. The theoretical values for C, H, and N for PIN1_2 agree well to the experimental ones with a maximal deviation of 8% for carbon. In contrast, the deviation for PIN1 and PIN2 is with 26 % and 21 % markedly larger. However, since we could not determine the composition of the sulphur-containing counter anion the theoretical values for the neutral polymers had to be used. Thus a comparison between theoretical and experimental compositions based on elemental analysis is flawed.

The nitrogen content of about 14 % is divided into three triazine nitrogen and one imine unit. This agrees the assumption that for each imine group one sulfur atom is incorporated into the network. This again supports the assumption of a sulfur containing counterion balancing the charge of the protonated imine. To best of our knowledge, the effect of protonation on an imine group due to the decomposition of DMSO has not yet been discussed in the current literature. Only few ionic microporous polymers are represented in the current literatur. Zhang *et al.* synthesized a tetrahedral network via homopolymerisation with a quaternary phosphonium cation in the center. This polymer displays high surface areas from 650-980 m^2g^{-1} which are tunable by changing the counteranions.[60] Further the quaternary pyridinium-type porous aromatic framework PAF-50 loaded with AgCl inside the pores was synthesized from the group around Zhu. This material is used for antibacterial performance and coatings.[61] Recently an anionic microporous organic polymer synthesised with a functionalised tetraphenylphosphonium ion was published. The ion exchange leads to an enhancement of the CO_2 uptake.[62]

With regard to the application of porous organic polymers, experimental data of the thermal stabilities under air are essential. Thermogravemetry analysis (TGA) show a good thermal stability of the polymers, with 10 % weight loss at temperature of 380 °C, 368 °C and 410 °C for PIN1, PIN2 and PIN1_2 respectively (Fig. 4). The negligible lower stability in contrast to other imine based polymers can be explained by the remained unreacted functional groups.

The broad X-ray diffraction pattern indicates an amorphous nature of the network (Fig. S5).

Table 2 CHNS chemical elemental composition (weight percentage). Calculated values assume complete conversion into the corresponding polymers (PIN1: $[C_{15}H_{10}N_2]^+$; PIN1_2: $C_{15}H_9N_2$ and PIN2: $[C_{57}H_{40}N_8]^{4+}$). Since we do not know the composition of the counteranion calculated values for PIN1 and PIN2 serve as estimates only.

Sample	C / %	H / %	N / %	S / %
PIN1				
Experimental	61.5	4.1	14.8	2.7
Calculated	82.6	4.6	12.8	-
PIN2				
Experimental	65.7	4.8	13.3	2.9
Calculated	82.2	4.3	13.5	-
PIN1_2				
Experimental	76.8	4.5	12.9	-
Calculated	82.9	4.2	12.9	-
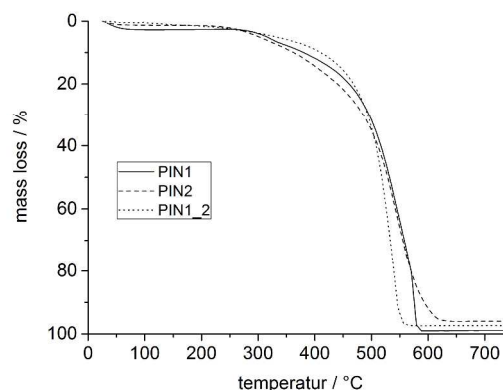
Fig. 4 Thermogravimetric analysis of PIN1, PIN2 and PIN1_2 under air.

Gas sorption properties

The porosity of PIN1, PIN2 and PIN1_2 was determined by argon measurements at 87 K (Fig. 5). To additionally determine ultramicropores, carbon dioxide isotherms were measured at 273 K (Fig. 8). The argon isotherms of PIN1 and PIN2 depicted in Fig. 5 can be assigned to type I (according to IUPAC classification) as well as to type IV. Both networks show a rapid gas uptake at low relative pressure ($p/p_0 < 0.05$), which indicates a predominant microporous structure. But the continual increase of the argon adsorption at relative high pressure ($p/p_0 = 0.1-0.9$) and the hysteresis are assigned to the presence of mesopores. Furthermore, it is noticeable that in both polymers the shape of the hysteresis is quite different. In PIN1 a hysteresis type H2 with a sharp step closure at a relative pressure about 0.4 is observable, which is an indication of an ink-bottle pore shape. The type H4 hysteresis in PIN2 is assigned to a slit pore dominated system. The reason for the differences might be a result of the different sterical demands of the monomers included in the networks. The hysteresis in the low pressure range of both networks is indicative for the presence of restricted-access pores[63] and to swelling of the network during the gas uptake. The latter one is probably also responsible for the small hysteresis observable for all CO_2 isotherms (Fig. 8).[64,65] Furthermore the isotherms at different temperatures show that the amount of adsorbed CO_2 increases with higher pressure and no saturation state which indicates a higher adsorption capacity towards higher pressure region.

Table 3 Specific surface areas and pore volumes derived from Ar (87 K) and CO_2 (273 K) sorption isotherms.

Sample	SA, $_{Ar, BET}$ / m^2 g^{-1}	SA$_{Ar, DFT}$ [a] / m^2 g^{-1}	SA, $_{CO2, DFT}$ [b] / m^2 g^{-1}	V$_{Ar, tot, DFT}$ /cm^3 g^{-1}	V$_{Ar, mic, DFT}$ / V$_{Ar, tot, DFT}$	V$_{CO2, tot, DFT}$ [d] /cm^3 g^{-1}
PIN1	458	409	411	0.30	0.50	0.12
PIN2	325	327	427	0.35	0.17	0.13
PIN1_2	28	23	245	0.05	-	0.08

[a]Ar using QSDFT for carbon material with cylindrical pores and adsorption branch (PIN1) or slit pores and equilibrium model (PIN2); [b] CO_2 isotherms at 273 K using a NLDFT slit pore model for carbon materials; [c] pore volume for pores with a diameter smaller than 2 nm calculated from an Ar QSDFT model for 87 K; [d] total pore volume for pores with a diameter smaller than 1 nm.

than 1 nm.
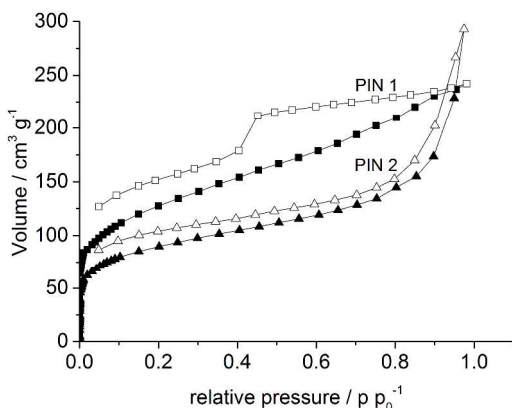
Fig. 5 Argon adsorption (filled symbols) and desorption (open symbols) isotherms at 87 K of PIN 1 and PIN2.

Applying the Brunner-Emmett-Teller (BET) method we estimated the surface areas (SA). The results are summarized in Table 3. The synthetic route in DMSO leads to moderate surface areas of 440 m^2 g^{-1} and 325 m^2 g^{-1} for PIN1 and PIN2, respectively. Whereas the polymer PIN1_2 synthesized in DMF exhibits only a low surface area of 30 m^2 g^{-1} estimated from the argon isotherm (Fig S6). Surprisingly, the surface area estimated from the CO_2 isotherms at 273 K (SA$_{CO2, DFT}$) of PIN1_2 is with a value of 245 m^2 g^{-1} significantly larger than the one measured with argon (Table 3). In the case of PIN2, the SA$_{CO2,DFT}$ of PIN2 is also 30 % higher than SA$_{Ar, DFT}$. An exception is PIN1. There the surface area of the CO_2 isotherm SA$_{CO2,DFT}$ is comparable to the isotherm of SA$_{Ar, DFT}$. These results demonstrate the presence of ultramicropores for PIN2 and PIN1_2 which are more easily accessible for CO_2 than for argon. This is caused on the higher kinetic energy of CO_2 at 273 K and the smaller kinetic diameter. These BET surface areas estimated from the argon isotherms are similar to values for other in DMSO synthesized imine polymers (MOP A-B1[50] 452 m^2 g^{-1}, C3V- POF[66] 438 m^2 g^{-1}, PSN-TAPA[67] 419 m^2 g^{-1}). Further imine based networks with higher surface areas were found (PI-1[40] 506 m^2 g^{-1}, COF 300[24] 1360 m^2 g^{-1}, POF[37] 1521 m^2 g^{-1}). The moderate surface areas from PIN1 and PIN2 might result from the incorporated counterions of the protonated imine units which partially block the pore volume. The pore size distributions (PSD) were obtained via the QSDFT or NLDFT methods applied on the argon and the carbon dioxide isotherms (Fig. 6 and Fig. 7). Due to the restriction in the used kernel for estimating PSDs the maximum pores which can be estimated from the CO_2 isotherms at 273 K have a diameter less
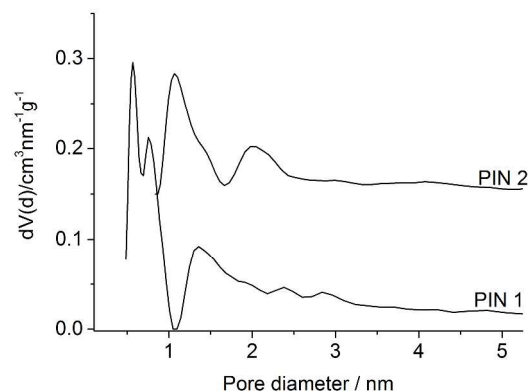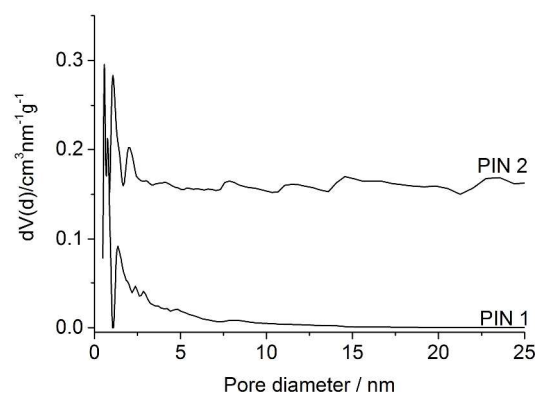
Fig. 6 (Top) Pore size distribution from the argon isotherm at 87 K of PIN1 and PIN2. The curves are shifted vertically by 0.15 cm^{3}nm^{-1}g^{-1} for clarity. (Bottom) Zoom in (0-5 nm) of the pore size distribution from the argon isotherm at 87 K of PIN1 and PIN2

In the PSDs calculated from the argon isotherms show a predominance of pores with a width of < 2nm. The main pore fraction of PIN1 is centering on 0.6 nm, which is commensurable with the PSD determined from the CO_2 isotherm. The PSD$_{Argon}$ from PIN1_2 show a very broad pore size distribution over the whole pore region (Fig S6). In contrast, the PSD$_{CO2}$ exhibit pores in the ultramicropore region. Furthermore for PIN1 and PIN2 also an amount of pores in the region between 2 nm and 5 nm are observable. Therefore, PIN1 and PIN2 display the presence of primary micropores and additional small mesopores.

Table 4: CO_2, N_2 and CH_4 uptakes of PIN polymers and heat of adsorption values

	CO_2 uptake[a] / mmol g^{-1}			Q_{st} / kJ mol^{-1}	N_2 uptake[a] / kJ mol^{-1}	CH_4 uptake[a] / kJ mol^{-1}	
	273 K	298 K	313 K		298 K	273 K	298 K
PIN1	1.80	1.22	0.99	31	0.07	0.46	0.29
PIN2	1.79	1.18	0.91	30	0.06	0.45	0.27
PIN1_2	1.06	0.70	0.57	30	-	0.25	0.13

[a] at 1 bar
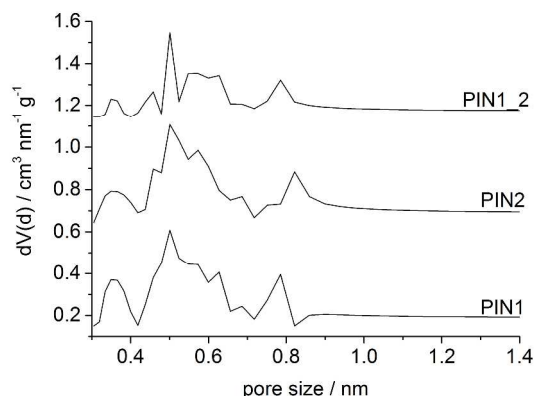
Fig. 7 Pore size distribution from carbon dioxide adsorption isotherms at 273 K using DFT calculations. The curves are shifted vertically by 0.5 cm^3 nm^{-1} g^{-1} for clarity.

The contribution of microporosity of the networks might be estimated as a ratio of $V_{Ar,mic,DFT}$ / $V_{Ar,tot,DFT}$ (Table. 3). PIN1 exhibits a value of 0.5 and PIN2 a value of 0.17. Predominantly micropores in PIN1 are observed, whereas the relative low value for PIN2 is explained by the existence of bigger mesopores. All polymers show similar pore sizes in the ultramicropore region (0.3-0.9 nm) due to the similar accessibility of CO_2 at 273 K. The differences are located in the micro- and mesopore character of the polymers.

Gas storage and selectivity

Additionally to the CO_2 isotherms of at 273 K further measurements at 298 K and 313 K for PIN1, PIN2 and PIN1_2 were done (Fig. 8). The absorption capacities for PIN1 and PIN2 with values up to 1.80 mmol g^{-1} at 273 K / 1bar (Table 4) are comparable to values determined for other Schiff base polymers such as CuPor-BPDC,[68] ILP,[69] MOP A-B1III [50] and ILCOF-1.[70] However the CO_2 uptake is considerably lower than in the imine linked PPF-1[71], triazine based frameworks,[72,73,74] microporous polyimide,[32,75] and benzimidazole-linked polymers BILP.[76,25,26] The CO_2 uptake values decrease with increasing temperature of about 34-20 %. Due to the significantly lower surface area and the absence of micropores in PIN1_2, the CO_2 uptakes of PIN1_2 are reduced by about 30 % compared to PIN1 and PIN2.

The moderate gas uptake capacity and moderate surface area of the synthesized networks might be an effect of the incorporated counterion of the protonated imine unit. This is responsible for blocking pore space and resulting in a hindered gas adsorption and diffusion. Additionally, the appearance of mesopores, which does not facilitate storage of small gases under low pressure, is

reducing the CO_2 uptake.[70] For determining the binding affinity, the isosteric heat of adsorption Q_{st} for CO_2 was calculated (Fig 9). The values given in Table 4 are estimated from the CO_2 uptake at the lowest measured loading. For PIN1, PIN2 and PIN1_2 adsorption enthalpies of around 30 kJ mol^{-1} could be determined. A decrease of all adsorption curves was observed, suggesting preferentially binding sites in the polymers. In spite of the different chemical structures and the ionic nature of PIN1, PIN2 compared to the neutral PIN1_2 all Q_{st} show similar values. Probably, this is caused by preferred adsorption of CO_2 into ultramicropores which show similar PSDs for all three networks (Fig. 7). In particular, Q_{st} values at low coverage (Table 4) are comparable to other polymers despite the relative low surface areas and moderate CO_2 uptakes.[7]

By using water vapour physisorption experiments we were able to examine the impact of the individual frameworks, on the water adsorption behaviour. The shape of the isotherms can be assigned to a type III after IUPAC classification (Fig S13). This indicates a weak interaction between the adsorbent and the water molecules.[77] PIN1 and PIN2 show similar shapes of the isotherms. In contrast, the slope of the adsorption branch of PIN1_2 is markedly smaller over the whole pressure region. For PIN1 and PIN2 the water vapour uptake at p/p$_0$ = 0.90 amounts to comparable values of 8.5 mmol g^{-1} and 7.0 mmol g^{-1}, respectively, while for PIN1_2 the same observable is with 3.0 mmol g^{-1} roughly three times lower. Due to their ionic nature PIN1 and PIN2 turn out to be highly polar and hydrophilic whereas the neutral PIN1_2 is more hydrophobic. This is also reflected in the selectivity coefficients of water over carbon dioxide. While as expected all three frameworks exhibit higher selectivities for water at room temperature (Table S2), again the neutral porous polymer PIN1_2 expresses a three times lower value of 27.

Furthermore, the adsorption selectivity of PIN1, PIN2 and PIN1_2 for CO_2 over N_2 and CH_4 were estimated based on the single-component gas adsorption isotherms of the three gasses. For this we rely on the ideal adsorbed solution theory (IAST)[78] and calculate the ratio of the initial slopes of adsorption isotherms in the Henry law region (<0.1 bar) (Table S3, Table S4, Table S5). Both methods are straightforward to use, however, neglect non-ideal behaviour and the presence of water vapour in targeted gas mixtures. In particular, the considerable high affinity of the frameworks towards water shown above might require removing water from any mixtures before using the materials as adsorbents and will probably lower the selectivity coefficients for CO_2 over N_2 and CH_4 obtained with IAST or the Henry method.[79] Selected estimated selectivities of CO_2/N_2 and CO_2/CH_4 derived from the IAST model are listed in Table. 5.
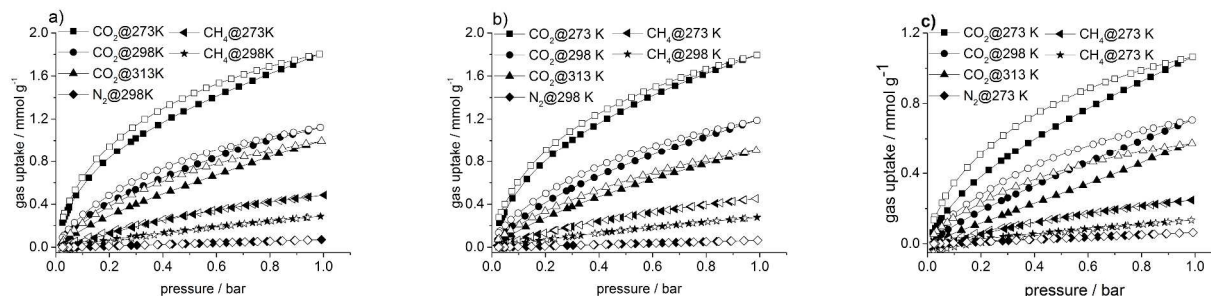
Fig 8 CO_2, CH_4 and N_2 adsorption (full symbols) and desorption (empty symbols) isotherms at 273 K, 298 K and 313 K from PIN1 (a), PIN2 (b) and PIN1_2 (c).

5 .
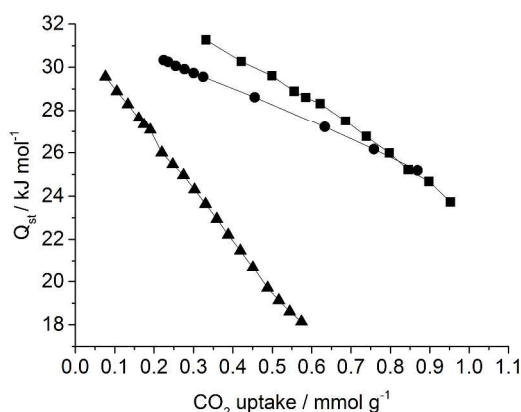
Fig 9 Isosteric heats of adsorption of CO_2 for PIN1 (quadrant), PIN2 (circle) and PIN1_2 (triangle) at different CO_2 loadings.

10 To model a typical fuel composition for a post-combustion process a mixture of 85 % N_2 and 15 % CO_2 at 298 K at atmospheric pressure were used for the calculations. The selectivities of the polymers for CO_2 over CH_4 were calculated at a typical feed composition for either natural gas with 5 % CO_2
15 and 95 % CH_4 or landfill gas with 50 % CO_2 and 50 % CH_4 (Table 5). PIN1 and PIN1_2 exhibit the same CO_2/N_2 selectivity factor of 30. These values are comparable with other imine based polymers (PAN-1: 35),[80] APOPs (31-20),[39] (PI-1: 27)[40] or other triazine based polymers (NOPs 39-26)[81] (NPTN 22-45)[82]
20 Nevertheless, these selectivity factors are lower than those of PCN-AD (112)[73] BILP-2 (113)[25] and MPI-1 (102).[75]

Table 5 Selectivities CO_2/N_2 and CO_2/CH_4 for PIN1, PIN2 and PIN1_2 at different temperatures.

	Selectivity CO_2/N_2 at 298 K	Selectivity CO_2/CH_4 at 273 K		Selectivity CO_2/CH_4 at 298 K	
Sample Ratio	$IAST^a$ 0.15/0.85	$IAST^b$ 0.05/0.95	0.5/0.5	$IAST^b$ 0.05/0.95	0.5/0.5
PIN1	31	12	4	8	5
PIN2	30	11	4	8	5
PIN1_2	-	8	5	7	6

^{a}calculated from IAST method as a specific 0.15/0.85 gas mixture at
25 298 K; ^{b}calculated from IAST method as a specific 0.05/0.95 or 0.5/0.5 gas mixture at 273 K or 298 K.

For PIN1_2 no calculation of the CO_2/N_2 selectivity was possible because of the very low N_2 loading. The predicted CO_2/CH_4 selectivities of the PINs for 05:95 mixtures in a natural gas
30 application are in a range of 8-12 (273 K) and 7-8 (298 K.) Meanwhile in a specified utilization of landfill gas (CO_2/CH_4 50:50) the values of the polymers are 5-4 (273 K) and 6-5 (298 K). These factors are comparable or only slightly lower to many other examples calculated with the IAST method such as
35 BILP-10 (9, ratio of 0.5/95 at 298 K),[83] PAN-2 (10, ratio of 0.5/95 at 298 K)[80], NPOF-4-NO_2 (11, ratio of 0.5/0.5 at 298 Å).[84] The analogousness of the selectivity values of PIN1 and PIN2 can be ascribed to the similar ultramicropore sizes, which is supported by the CO_2 uptakes, surface areas and heat of
40 adsorption calculated from CO_2 isotherms.

In all polymers different molar ratios of CO_2/CH_4 result in different selectivity behavior with increasing pressure (Figs 10 and S30 – S32). A higher content of CO_2 in the gas mixture leads to a decrease of the selectivity with increasing pressure, whereas
45 a lower content of CO_2 in the mixture results in an increase of the selectivity factor. The reason for that is a specific adsorption of CO_2 at low pressure in ultramicropores which are not accessible for CH_4. With higher pressure the small pores are filled continuously and adsorption of bigger pores also with CH_4 starts.
50 Due to the low amount of CO_2 in the 05:95 mixture, it is not possible to fill all accessible ultramicropores over the whole pressure region. Therefore, specific adsorption sites are still available and CO_2 not competing with CH_4 even at higher pressure, this result in an increase of the selectivity. This effect is
55 less pronounced for the CO_2/N_2 selectivity (Figs 10 and S29). The selectivities in both polymers decrease with raising pressure, independent of the composition of the gas mixture. The difference in the behaviour of the selectivity is attributed to the different kinetic diameters of CH_4 (3.80 Å) and N_2 (3.64 Å)[85].
60 The smaller diameter of N_2 allows molecules to enter pores sizes, which are not accessible for CH_4. Hence a higher competition with CO_2 for adsorption in small pores is the consequence. But it has to be noted, that the absolute selectivity values for CO_2/CH_4 are much lower than those of CO_2/N_2. Besides kinetic
65 factors which lead to a sieving effect, also the dipole moment and thermodynamic factors should be taken into account. The localized dipoles of the N-containing groups and the high quadrupole moment of CO_2 (CO_2 $14.3 \cdot 10^{-40}$ cm^2, N_2 $4.65 \cdot 10^{-40}$ cm^2, CH_4 none)[86] leads to a strong interaction between gas and

network.[87] Additionally, the lower selective adsorption of CO_2 over CH_4 in comparison over N_2 can be explained by the differences in the thermodynamic factors. The critical temperature of CO_2 (304 K) is much higher than that of N_2 with 126.2 K and CH_4 with 191.6 K. [88]
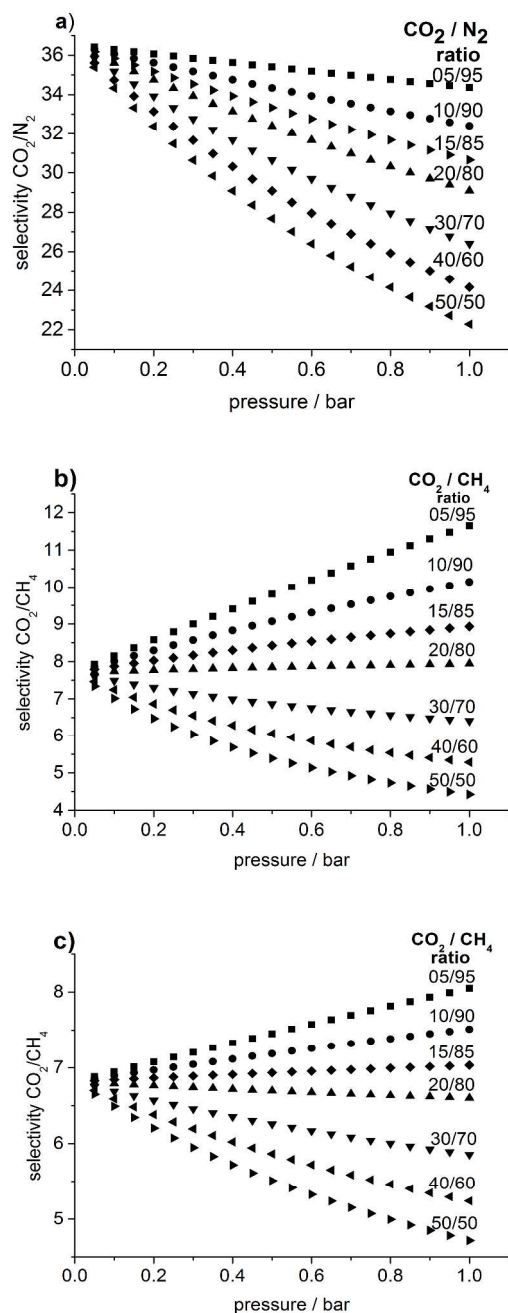
Fig 10 IAST selectivities for CO_2/N_2 (a) and CO_2/CH_4 at 273 K (b) and 298 K (c) of PIN1

Conclusion

We have successfully synthesized porous polymer networks PIN1 and PIN2 through Schiff base chemistry under catalyst-free conditions in DMSO. The synthesis in DMF only results in a non porous network, according to argon isotherms (PIN1_2). We expect that the main driving force for the pore formation is based on the structural rigidity due to the generation of free volume. This is achieved by using monomers 9,10-anthracene-dicarboxaldehyde or tetrakis(4-formylphenyl)methane. The successful introduction of different functional groups, such as triazine units, which are contained in 4,6-tris(4-aminophenyl)-1,3,5-triazine and imine units were confirmed by ^{13}C and ^{15}N NMR and infrared spectroscopic measurements. IR and ^{15}N NMR measurements reveal a protonation of the imine unit most likely due to the decomposition of DMSO. The produced acid leads to an ionic structure of the polymers with a sulfonic counterion. Because of the ionic behaviour, additionally to the incorporated polar groups such as triazine and imine functions, the materials are interesting to investigate about their gas storage and selectivity properties.

All polymers have an amorphous nature and exhibit good thermal stability up to 400 °C. Moderate surface areas of 458 $m^2\,g^{-1}$ and 325 $m^2\,g^{-1}$ were attained for PIN1 and PIN2, respectively. Whereas PIN1_2, polymerized in DMF instead of DMSO show no porosity calculated from the argon isotherm at 87 K. Therefore, the high influence of the solvent on the generation of pores is verified. The moderate surface areas for PIN1 and PIN2 are reasoned by pore blocking of embedded counterions. Pore size distributions for both networks show micro- and mesopores for both polymers, with pore sizes between 0.3 and 5 nm. All polymers exhibit high isosteric heats of adsorption at low coverage of around 30 kJ mol^{-1}. This is attributed to the presence of Lewis basic acceptor groups which result in a strong dipole-quadrupole interaction of the surface and CO_2 molecules. This leads to CO_2 uptake capacities at 1.0 bar and 273 K of 1.8 mmol g^{-1} for PIN1 and PIN2 and 1.06 mmol g^{-1} for PIN1_2. The good uptake of CO_2 in contrast to the moderate surface areas is based on the better accessibility of CO_2 into the narrow micropores than for argon. Water vapour measurements also support a more hydrophilic, polyionic nature of PIN1 and PIN2 compared to the neutral PIN1_2. This is reflected by an increase of both the water uptake and the water selectivity over carbon dioxide by roughly a factor of three from the neutral to the polyionic networks. The high water uptake for PIN1 and PIN2 implies a different water sorption mechanism. Whereas water adsorbed in PIN1_2 competes with carbon dioxide for polar binding sites on the framework, the uptake of water in PIN1 and PIN2 might lead to a protonation of water from the protonated imine linkages which would explain the much higher affinity for water for these two frameworks.

The CO_2/N_2 selectivities for PIN1 and PIN2 at 298 K and 1 bar were found to be 30, comparable with other porous imine polymers. Furthermore, all polymers display very good selectivities for CO_2 over CH_4 of 12-8 at 273 K and 8-7 at 298 K, both at 1 bar. Noticeable the selectivities show strong molar ratio dependence. Despite the relative low surface area and moderate CO_2 uptake comparably good selectivity factors have been achieved. The above results indicate potential materials for capture CO_2 in the environmental-protection fields.

Acknowledgments

Notes and references

[a] Department for Inorganic Chemistry III, University of Bayreuth, Universitätstr. 30, 95440 Bayreuth, Germany;
E-mail: juergen.senker@uni-bayreuth.de
[b] Institute of Inorganic Chemistry, Christian-Albrechts-University Max-Eyth-Straße 2, 24118 Kiel, Germany

† Electronic Supplementary Information (ESI) available: [NMR and IR spectra, XRD pattern, BET plots, DFT fitting data for argon and CO_2 sorption isotherms and Langmuir fit data]. See DOI: 10.1039/b000000x/ DOI: 10.1039/b000000x/ DOI: 10.1039/b000000x/

1 K. M. Kerry Yu, I. Curcic, J. Gabriel, S. C. E. Tsang, *ChemSusChem,* 2008, **1**, 893-899.

2 R. S. Haszeldine, *Science*, 2009, **325**, 1647-1652.

3 Z. Zhang, Y. Zhao, Q. Gong, Z. Li, J. Li, *Chem Commun*, 2013, **49**, 653-661.

4 F. M. Orr, Jr., Energy *Environ. Sci.*, 2009, **2**, 449-458.

5 D. M. D'Alessandro, B. Smit, J. R. Long, *Angew. Chem .Int. Ed, 2010,* **49**, 6058–6082.

6 C. Xu, N. Hedin, *Materials Today*, 2014, **17**, 397-403.

7 R. Dawson, A. I. Cooper, D. J. Adams, *PolymInt*, 2013, **62**, 345-352.

8 S. Cavenati, C.A. Grande, A.E. Rodrigues, *Energy&Fuels*, 2006, **20**, 2648-2659.

9 G. T. Rochelle, *Science, 2009,* **325**, 1652–1654.

10 A. Yamasaki, *J. Chem. Eng. Jpn*. 2003, **36**,361-375.

11 J. T. Yeh, K. P. Resnik, K. Rygle, H. W. Pennline, *Fuel Process. Technol.*, 2005, **86**, 1533-1546.

12 X. Xu, C. S. Song, J. M. Andresen, B. G. Miller, A. W. Scaroni, *Energy&Fuels*, 2002, **16**, 1463-1469.

13 M. S. Shafeeyan, W. M. A. W. Daud, A. Houshmand, A. Shamiri, *J. Anal. Appl. Pyrol.*, 2010, **89**, 143–151.

14 A. Samanta, A. Zhao, G. K. H. Shimizu, P. Sarkar, R. Gupta, *Ind. Eng. Chem. Res*., 2012, **51**, 1438–1463.

15 O. Cheung, N. Hedin*, RSC Adv*., 2014, **4**, 14480–14494.

16 J-R. Li, J. Sculley, H-C. Zhou, *Chem.Rev*., 2012, **112**, 869-932.

17 K. Sumida, D. L. Rogow, J. A. Mason, T.M. McDonald, E. D. Bloch, J. R. Herm, T-H. Bae, J. R. Long, *Chem. Rev*., 2012, **112**, 724-781.

18 J-R. Li, Y. Ma, M. C. McCarthy, J. Sculeey, J. Yu, H.-K. Jeong, P. B. Balbuena, H.-C. Zhou, Coord*. Chem. Rev*., 2011, **255**, 1791-1823.

19 R. Dawson, A. I. Cooper, D. J. Adams, *Prog. Polym. Sci.*, 2012, **37**, 530-563.

20 R. Dawson, E. Stöckel, J. R. Holst, D. J. Adams, A. I. Cooper, *Energy Environ. Sci,* 2011, **4**, 4239.

21 P. Katekomol, J. Roeser, M. Bojdys, J. Weber, A. Thomas, *Chem. Mater.,* 2013, **25**, 1542-1548.

22 P. Kuhn, M. Antonietti, A.Thomas*, Angew.Chem*., 2008, **120**, 34969-3502.

23 H. Furukawa, O. M. Yaghi, *J. Am. Chem. Soc*., 2009, **131**, 8875-8883.

24 F. J. Uribe-Romo, J. R. Hunt, H. Furukawa, C. Kloeck, M. O`Keeffe, O. M. Yaghi, *J. Am. Chem. Soc*., 2009, **131**, 4570-4571.

25 M. G. Rabbani, H. M. El-Kaderi, *Chem. Mater*., 2012, **24**, 1511-1517.

26 M. G. Rabbani, A. K. Sekizkardes, O. M. El-Kaderi, B. R. Kaafarani, H. M. El-Kaderi*, J. Mater. Chem*., 2012, **22**, 25409-25417.

27 N. B. McKeown, P.M. Budd, *Chem. Soc. Rev*., 2006, **35**, 675-683.

28 N. B. McKeown, P. M. Budd, *Macromolecule*s, 2010, **43**, 5163-5176.

29 Q. Chen, M. Luo, P. Hammershoj, D. Zhou, Y. Han, B.W. Laursen, C. G. Yan, B. H. Han, *J. Am. Chem. Soc*.,2012, **124**, 6084-6087.

30 X. Zhu, S. M. Mahurin, S.-H. An, C.-L. Do-Thanh, C. Tian, Y. Li, L. W. Gill, E. W. Hagaman, Z. Bian, J.-H. Zhou, J. Hu, H. Liu, S. Dai, *Chem. Commun.,* 2014, **50**, 7933-7936.

31 J. Weber, M. Antonietti, A. Thomas*, Macromolecules*, 2008, **41**, 2880-2885.

32 M. R. Liebl, J. Senker, *Chem. Mater*., 2013, **25**, 970-980.

33 O. K. Farha, A. M. Spokoyny, B. G. Hauser, Y.-S. Bae, S.E. Brown, R. Q. Snurr, C. A. Mirkin, J. T. Hupp, *Chem. Mater*., 2009, **21**, 3033-3035.

34 H. A. Patel, S. H. Je, J. Park, D. P. Chen, Y. Jung, C. T. Yavuz, A. Coskun*, Nat. Commun*., 2013, **4**, 1357.

35 J. Lu, J. Zhang, *J. Mater. Chem. A*., 2014, **2**, 13831-13834.

36 Y. Jin, Y. Zhu, W. Zhang, *CrystEngComm*, 2013, **15**, 1484–1499.

37 P. Pandey, A.P. Katsoulidis, I. Eryazici, Y. Wu, M.G. Kanatzidis, S.T. Nguyen, *Chem Mater*., 2010, **22**, 4974-4979.

38 M. G. Schwab, B. Fassbender, H. W. Spiess, A. Thomas, X. Feng, K. Müllen, *J. Am. Chem. Soc*., 2009, **131**, 7216–7217.

39 W.-C. Song, X.-K. Xu, Q. Chen, Z.-Z. Zhuang, X.-H. Bu, *Polym. Chem*., 2013, **4**, 4690-4696.

40 A. Laybourn, R. Dawson, R. Clowes, J. A. Iggo, A. I. Cooper, Y. Z. Khimyak, D. J. Adams, *Polym. Chem*., 2012, **3**, 533-537.

41 L. Liu, P.-Z. Li, L. Zhu, R. Zou, Y. Zhao, *Polymer,* 2013, **54**, 596-600.

42 S. Ren, R. Dawson, A. Laybourn, J.-X Jiang, Y. Khimyak, D.J. Adams, A. I. Cooper, *Polym. Chem*., 2012, **3**, 928-934.

43 J. Rouquerol, P. Llewellyn, F. Rouquerol, *Stud. Surf. Sci. Catal*., 2007, **160**, 49-56.

44 B.M. Fung, A. K. Khitrin, K. Ermolaev*, J. Magn. Reson*., 2000, **142**, 97-100.

45 K. R. Idzik, P. Ledwon, R. Beckert, S. Golba, J. Frydel, M. Lapkowski, *Electrochimica Acta*, 2010, **55**, 4858-4864.

46 T. Ishi-I, R. Kuwahara, A. Takata, Y. Jeong, K. Sakurai, S. Mataka*, Chem. Eur. J*., 2006, **12**, 793-776.

47 A. E. Lee, M. R. Grace, A. G. Meyer, K. L. Tuck, *Tetrahedron Letters,* 2010, **51**, 1161-1165.

48 W. Lu, D. Yuan, D. Zhao, C. I. Schilling, O. Plietzsch, T. Muller, S. Brase, J. Guenther, J. Blumel, R. Krishna, *Chem. Mater.,* 2010, **22**, 5964-5972.

49 X. Li, B.C. Gibb, *Supramol. Chem*, 2003, **15**, 495-504.

50 C. Xu, N. Hedin, *J. Mater. Chem. A*, 2013, **1**, 3406-3414.

51 C. Mésangeau, S. Yous, B. Pérès, D. Lesieur, T. Besson, *Tetrahedron Lett*., 2005, **46**, 2465-2468.

52 D. L. Head, C. G. McCarty, *Tetrahedron Lett*., 1973, **16**, 1405-1408.

53 P. Kuhn, A. Thomas, A. Antonietti, *Macromolecules*, 2009, **42**, 319-326.

54 M. J. Bojdys, J. Jeromenok, A. Thomas, M. Antonietti, *Adv. Mater*., 2010, **22**, 2202-2205.

55 V. G. Manecke, D. Wöhrle, *Makromol. Chem.,* 1968, **120**, 176-191.

56 S. Hug, M. B. Mesch, H. Oh, N. Popp, M. Hirscher, J. Senker, B. V. Lotsch, *J. Mater. Chem*., 2014, **2**, 5928.

57 J. Wang, I. Senkovska, M. Oschatz, M. R. Lohe, L. Borchardt, A. Heerwig, Q. Liu, S. Kaskel, *J. Mater. Chem. A*., 2013, **1**, 10951-10961.

58 F. M. Wisser, K. Eckhardt, D. Wisser, W. Böhlmann, J. Grothe, E. Brunner, S. Kaskel, *Macromolecules*, 2014, **47**, 4210-4216.

59 V. J. Traynelis, W. L Hergenrother, *J. Org. Chem*., 1964, **29**, 221-222.

60 Q. Zhang, S. Zhang, S. Li, Macromolecules, 2012, 45, 2981-2988.

61 Y. Yuan, F. Sun, F. Zhang, H. Ren, M. Guo, K. Cai, X. Jing, X. Gao, G. Zhu, *Adv. Mater*., 2013, **25**, 6619-6624.

62 S. Fischer, A. Schimanowitz, R. Dawson, I. Senkovska, S. Kaskel, A. Thomas, *J. Mater. Chem. A*, 2014, **2**, 11825-11829.

63 J. Jeromenok, J. Weber, *Langmuir* 2013, **29**, 12982-12989.

64 C. Serre, S. Bourrelly, A. Vimont, N. A. Ramsahye, G. Maurin, P. L. Llewellyn, M. Daturi, Y. Filinchuk, O. Leynaud, P. Barnes, G. Férey, *Adv. Mater.,* 2007, **19**, 2246–2251.

65 C. Li, W. Qiu, W. Shi, H. Song, G. Bai, H. He, J. Lia, M. J. Zaworotkoc, *CrystEngComm*, 2012, **14**, 1929–1932.

66 E. Verde-Sesto, E. M. Maya, Á. E. Lozano, J. G. de la Campa, F. Sánchez, M. Iglesias, *J. Mater. Chem.*, 2012, **22**, 2437-24643.

67 G. Li, B. Zhang, J. Yan, Z. Wang, *J. Mater. Chem.,* 2014, **2**, 18881-18888.

68 V. S. P. K. Neti, X. Wu, S. Deng, L. Echegoyen, *Polym. Chem.*, 2013, **4**, 4566-4569.

69 J. Wang, I. Senkovska, M. Oschatz, M.R. Lohe, L. Borchardt, A. Heerwig, Q. Liu, S. Kaskel, *ACS Appl. Mater. Interfaces,* 2013, **5**, 3160- 3167.

70 M. G. Rabbani, A. K. Sekizkardes, Z. Kahveci, T. E. Reich, R. Ding, H. M. El-Kaderi, *Chem. Eur. J.*, 2013, **19**, 3324-3328.

71 Y. Zhu, H. Long, W. Zhang, *Chem. Mater.* 2013, **25**, 1630-1635.

72 W. Wang, H. Ren, F. Sun, K. Cai, H. Ma, J. Du, H. Zhao, G. Zhu, *Dalton Trans.*, 2012, **41**, 3933-3936.

73 C. Shen, H. Yu, Z. Wang, *Chem. Commun.*, 2014, **50**, 11238-11241.

74 A. Bhunia, I. Boldog, A. Möller, C. Janiak, *J. Mater. Chem. A.*, 2013, **1**, 14990-14999.

75 G. Li, Z. Wang, *Macromolecules* 2013, **46**, 3058-3066.

76 M. G. Rabbani, H. M. El-Kaderi*, Chem. Mater.*, 2011, **23**, 1650-1653.

77 M. Rose, N. Klein, I. Senkovska, C. Schrage, P. Wollmann, W. Böhlmann, B. Böhringer, S. Fichtner, S. Kaskel, *J. Mater. Chem.*, 2011, **21**, 711-716.

78 A. L Meyers, J. M Prausnitz, *A.I.Ch.E.J.*, 1965, **11**, 121-127.

79 R. Dawson, L. A. Stevensen, T. C. Drage, C. E. Snape, M. W. Smith, D. J. Adams, A. I. Cooper, *J. Am. Chem. Soc.,* 2012, **134**, 10741-17744.

80 G. Li, B. Zhang, J. Yan, Z. Wang, *Macromolecules,* 2014, **47**, 6664-6670.

81 S. Xiong, X. Fu, L. Xiang, G. Yu, J. Guan, Z. Wang, Y. Du, X. Xiong, C. Pan, *Polym. Chem,.* 2014, **5**, 3424-3431.

82 S. Wu, Y. Lui, G. Yu, J. Guan, C. Pan, Y. Du, X. Xiong, Z. Wang, *Macromolecules,* 2014, **47**, 2875-2882.

83 A. K. Sekizkardes, T. İslamoğlu, Z. Kahveci, H. M. El-Kaderi, *J. Mater. Chem. A*, 2014, **2**, 12492–12500.

84 T. İslamoğlu, M G. Rabbani, H. M. El-Kaderi, *J. Mater. Chem.*, 2013, **1**, 10259-10266.

85 T. E. Rufford, ,S. Smart, C. C. Y. Watson, B. F. Graham, J. Boxhall, J. C. Diniz da Costa, E. F. May, *J. Petrol. Sci. Eng.,* 2012, **94-94**, 123-154.

86 C. Graham, D. A. Imrie, R. E. Raab, *Mol. Phys.*, 1998, **93**, 49-56.

87 Z. Zhang, Y. Zhao, Q. Gong, Z. Li, J. Li, *Chem. Commun.*, 2013, **49**, 653-661.

88 J. Jeans *An Introduction to the Kinetic Theory of Gases*; Cambridge University Press: London, 1982.

Porous imine-linked networks with protonated imine linkages and an ionic structure were synthesized. They exhibit good carbon dioxide uptakes and CO_2/N_2 as well as CO_2/CH_4 separation coefficients.